SCIENCE CHINA
Information Sciences

• RESEARCH PAPER •

February 2024, Vol. 67, Iss. 2, 122403:1–122403:12
https://doi.org/10.1007/s11432-022-3618-3

Experimental and numerical demonstration of hierarchical time-delay reservoir computing based on cascaded VCSELs with feedback and multiple injections

Xingxing GUO[1], Shuiying XIANG[1,2*], Xingyu CAO[1] & Biling GU[1]

[1]*State Key Laboratory of Integrated Service Networks, Xidian University, Xi'an* 710071*, China;*
[2]*State Key Discipline Laboratory of Wide Bandgap Semiconductor Technology, School of Microelectronics, Xidian University, Xi'an* 710071*, China*

Received 27 April 2022/Revised 20 August 2022/Accepted 11 November 2022/Published online 30 October 2023

Abstract In this paper, we propose and demonstrate experimentally and numerically a hierarchical time-delay optical reservoir computing (RC) system based on cascaded vertical-cavity surface-emitting lasers (VCSELs) with feedback and multiple injections. The prediction performance characteristics of the hierarchical time-delay RC system based on cascaded VCSELs under different reservoir layers are compared. Evidently, the prediction performance of the hierarchical time-delay RC system is first improved and saturates as the number of reservoir layers increases. Besides, the impacts of key factors on predicting the hierarchical time-delay RC system are also analyzed in detail experimentally and numerically. This proposed hierarchical time-delay RC system based on VCSELs is useful for the further development of RC systems and may be beneficial to improve the ability of RC systems to solve more complex problems.

Keywords vertical-cavity surface-emitting laser, reservoir computing, neuromorphic photonics, time-delay system, information processing

1 Introduction

In the current information age, the amount of information has exploded. Therefore, finding fast and efficient information processing methods has become a general trend [1–3]. Reservoir computing (RC) is a neuromorphic computing framework similar to human cortical circuits and suitable for processing timing signals [3–6]. RC is derived from several recurrent neural network models, including echo state networks and liquid state machines [7, 8]. Generally, RC systems include a reservoir layer for mapping inputs to high-dimensional space and an output layer for pattern analysis from high-dimensional states in the reservoir layer [9]. Compared with the software implementation on traditional electronic computers, the realization of the RC based on optical devices has significant advantages, such as ultrahigh speed and ultralow power consumption [10].

The RC hardware system based on a single delay feedback nonlinear dynamic system (referred to as the time-delay RC) has attracted widespread attention due to its simple structure [11–16]. In the delay feedback loop, virtual nodes are set up to replace the large-scale nodes in the traditional reservoir according to the idea of time division multiplexing, which greatly simplifies the hardware implementation structure of the RC system [11].

The vertical-cavity surface-emitting laser (VCSEL) is a new type of semiconductor laser that emits light on a vertical surface [17]. Compared with the traditional edge-emitting lasers, VCSELs can easily be integrated into two dimensions and have a low threshold, low cost, advanced technology, and rich polarization dynamics characteristics [18–20]. To date, VCSELs have been successfully applied in optical storage, optical recognition, parallel optical processing, and optical interconnection systems [21].

* Corresponding author (email: jxxsy@126.com)

Recently, using the VCSEL as a nonlinear node in the time-delay RC system has been proposed and received extensive attention [22–26]. In 2018, Vatin et al. [22] novelly proposed a time-delay optical RC system based on a VCSEL subject to feedback and optical injection. The numerical results demonstrated that compared to the case with only a polarization mode in the VCSEL, when two polarization modes in the VCSEL coexisted, the RC system had higher computing performance, larger memory capacity, and better classification capabilities. In 2019, they further experimentally realized that such time-delay optical RC system was based on the VCSEL, proving once again that the RC system performed better when two polarization modes coexisted in the VCSEL [23]. In the same year, Guo et al. [24] proposed using two polarization modes in the VCSEL to achieve parallel task processing in a time-delay optical RC system based on a single VCSEL with polarization feedback. Through numerical analysis, the RC system successfully completed the chaotic time series prediction and waveform recognition tasks in parallel for two different feedback structures. In 2020, Guo et al. [25] further proposed a four-channel time-delay optical RC system based on mutually coupled VCSELs. Here, four channels were novelly implemented in two polarization modes in two VCSELs. It was found that the four-channel RC could produce better prediction performance and faster information processing rate compared to the one-channel RC system. Note that most studies on time-delay optical RC systems based on VCSELs are concentrated in a single reservoir layer structure (shallow structure), indicating that there is only the time depth but no depth in space in such a system. However, the limitations of the short-term memory ability and complex dynamic characteristics of the single reservoir layer structure fundamentally restrict the improvement of the information processing capability of the RC system. Especially, the hierarchical reservoir layer structure has not been applied to the RC system based on the VCSEL so far, which is worthy of further exploration for improving the RC performance.

Herein, we combine the VCSEL-based time-delay optical RC system and hierarchical structure and propose a hierarchical time-delay optical RC system based on cascaded VCSELs with feedback and multiple injections. Such a hierarchical time-delay optical RC system comprises stacked multiple reservoir layers between the input and output layers. The remainder of this paper is structured as follows. Section 2 describes the system design of a hierarchical time-delay optical RC system based on cascaded VCSELs and introduces the rate equation model in detail. Section 3 numerically verifies and compares the prediction performance of the hierarchical time-delay optical RC system based on cascaded VCSELs under different reservoir layers. Then the influences of the coupling strength, the feedback strength, the spontaneous emission noise, and the number of reservoir layers are considered. Furthermore, Section 4 proposes an experimental scheme of the hierarchical time-delay RC system with two reservoir layers. Next, the effect of the coupling power and the power of the external input signal are considered. Finally, Section 5 concludes the study.

2 Theory and model

The schematic of the proposed hierarchical time-delay RC system based on cascaded VCSELs with feedback and multiple injections is displayed in Figure 1. In such a hierarchical time-delay RC system, one reservoir layer is realized by a single VCSEL with feedback. The output of the previous VCSEL and the external input signal are injected into the VCSEL of the next reservoir layer together. Next, the output of the last VCSEL can be extracted for post-processing. Here, a hierarchical time-delay RC system based on a cascaded VCSEL with four reservoir layers is taken as an example. For each reservoir layer, the number of virtual nodes is Z, and the interval between the adjacent virtual nodes is θ. Additionally, the binary mask signal $(-1,\ 1)$ is used for the hierarchical time-delay RC system based on cascaded VCSELs [27, 28].

In the multiple reservoir layers of the proposed hierarchical time-delay RC system, four VCSELs with feedback and unidirectional coupling under external optical injection are considered. The rate equations used for the hierarchical RC system are derived based on the well-known spin-flip model, and can be expressed as [29–33]:

$$\begin{aligned}\frac{\mathrm{d}E_{1x}}{\mathrm{d}t} =& \kappa(1+\mathrm{i}\alpha)\left(N_1E_{1x}-E_{1x}+\mathrm{i}nE_{1y}\right)-\left(\gamma_a+\mathrm{i}\gamma_p\right)E_{1x}\\ &+k_{d1}E_{1x}\left(t-\tau_{d1}\right)\exp\left(-\mathrm{i}\omega_{x1}\tau_{d1}\right)+k_{\mathrm{inj}1}\varepsilon(t)+F_{x1},\end{aligned}\tag{1}$$

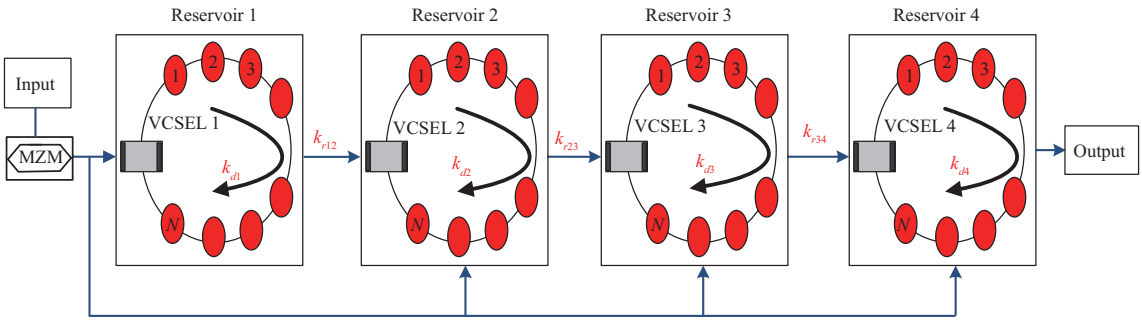

Figure 1 (Color online) Schematic diagram of a hierarchical time-delay RC system based on cascaded VCSELs with four reservoir layers.

$$\begin{aligned}\frac{\mathrm{d}E_{1y}}{\mathrm{d}t}=&\kappa(1+\mathrm{i}\alpha)\left(N_1E_{1y}-E_{1y}+\mathrm{i}n_1E_{1x}\right)-\left(\gamma_a+\mathrm{i}\gamma_p\right)E_{1y}\\&+k_{d1}E_{1y}\left(t-\tau_{d1}\right)\exp\left(-\mathrm{i}\omega_{y1}\tau_{d1}\right)+F_{y1},\end{aligned}\tag{2}$$

$$\begin{aligned}\frac{\mathrm{d}E_{1y}}{\mathrm{d}t}=&\kappa(1+\mathrm{i}\alpha)\left(N_1E_{1y}-E_{1y}+\mathrm{i}n_1E_{1x}\right)-\left(\gamma_a+\mathrm{i}\gamma_p\right)E_{1y}\\&+k_{d1}E_{1y}\left(t-\tau_{d1}\right)\exp\left(-\mathrm{i}\omega_{y1}\tau_{d1}\right)+F_{y1},\end{aligned}\tag{3}$$

$$\begin{aligned}\frac{\mathrm{d}E_{my}}{\mathrm{d}t}=&\kappa(1+\mathrm{i}\alpha)\left(N_mE_{my}-E_{my}+\mathrm{i}n_mE_{mx}\right)-\left(\gamma_a+\mathrm{i}\gamma_p\right)E_{my}\\&+k_{cm}E_{my}\left(t-\tau_{cmn}\right)\exp\left(-\mathrm{i}\omega_{ym}\tau_{cmn}\right)\\&+k_{r(m-1)m}E_{(m-1)y}\left(t-\tau_{(m-1)m}\right)\mathrm{e}^{-\mathrm{i}\omega_{y(m-1)}\tau_{(m-1)m}}\mathrm{e}^{\mathrm{i}\Delta\omega_{y(m-1)m}t}+F_{ym},\end{aligned}\tag{4}$$

$$\begin{aligned}\frac{\mathrm{d}N_{1,m}}{\mathrm{d}t}=&\gamma_N\left[\mu_{1,m}-N_{1,m}\left(1+\left|E_{1x,mx}\right|^2+\left|E_{1y,my}\right|^2\right)\right.\\&\left.+\mathrm{i}n_{1,m}\left(E_{1x,mx}E_{1y,my}^*-E_{1y,my}E_{1x,mx}^*\right)\right],\end{aligned}\tag{5}$$

$$\begin{aligned}\frac{\mathrm{d}n_{1,m}}{\mathrm{d}t}=&-\gamma_sn_{1,m}-\gamma_n\left[n_{1,m}\left(\left|E_{1x,mx}\right|^2+\left|E_{1y,my}\right|^2\right)\right.\\&\left.+\mathrm{i}N\left(E_{1y,my}E_{1x,mx}^*-E_{1x,mx}E_{1y,my}^*\right)\right],\end{aligned}\tag{6}$$

where $E_{1x,mx}$ and $E_{1y,my}$ are the slowly varied complex field amplitudes of two polarization modes of VCSELs. The difference between carrier inversions with opposite spins is $n_{1,m}$, and the total carrier inversion between conduction and valence bands is $N_{1,m}$. The subscript 1 represents VCSEL1, m ($m=2,3,4$) represent VCSEL2, VCSEL3, VCSEL4, and x and y represent x-polarization (XP) and y-polarization (YP) modes of VCSEL, respectively. $\mu_{1,m}$ stand for the normalized bias current of the four VCSELs, and $\mu_{1,m}=\mu$. Besides, κ is the field decay rate, α stands for the linewidth enhancement factor, γ_N is the decay rate of $N_{1,m}$, and γ_s is the spin-flip rate. γ_a represents the linear dichroism, and γ_p expresses the linear birefringence. The third term in (1)–(4) represents the feedback term, where the feedback strength is $k_{d1,dm}$, and the feedback delay is $\tau_{d1,dm}$ [33].

The fourth term in (1) and (3) represents the external optical injection item, $k_{\mathrm{inj1,inj}m}$ represents the external optical injection strength. $\varepsilon(t)$ stands for the output of Mach-Zehnder modulator (MZM), and $\varepsilon(t)=\frac{|\varepsilon_0|}{2}\{1+\mathrm{e}^{\mathrm{i}[S(t)+\Phi_0]}\}\mathrm{e}^{\mathrm{i}2\pi\Delta f_st}$ [34]. The masked input signal $S(t)$ is injected into the four VCSELs through four MZMs, and the frequency detuning between the XP mode of VCSEL and the injected field is uniformly set to be Δf_s. Here, $|\varepsilon_0|$ is the injection field amplitude. Φ_0 is the bias voltage of the MZM. The fifth (sixth) term in (3) (Eq. (4)) is the unidirectional coupling term. The coupling strength is $k_{r(m-1)m}$, and the coupling delay is $\tau_{(m-1)m}$. The last term in (1)–(4) represents the spontaneous emission noise simulated by Langevin source [19], and $F_{x1,xm}=\sqrt{\beta_{x1,xm}/2}(\sqrt{N+n}\xi^{x1,xm}+\sqrt{N-n}\xi^{x1,xm})$, $F_{y1,ym}=-\mathrm{i}\sqrt{\beta_{y1,ym}/2}(\sqrt{N+n}\xi^{y1,ym}-\sqrt{N-n}\xi^{y1,ym})$. $\beta_{x1,xm}$ and $\beta_{y1,ym}$ are the intensity of spontaneous emission. $\xi^{x1,xm}$ ($\xi^{y1,ym}$) is an independent Gaussian white noise source with variance of 1 and mean of 0.

For simplicity, we consider the case where the feedback strength, feedback delay, and coupling strength of the four VCSELs are equal, that is $k_{d1}=k_{dm}=k_d$, $\tau_{d1}=\tau_{dm}=\tau_d$, $\tau_{(m-1)m}=\tau$, $k_{r(m-1)m}=k_r$, $k_{\mathrm{inj1}}=k_{\mathrm{inj}m}=k_{\mathrm{inj}}$, $\beta_{x1,xm}=\beta_{y1,ym}=\beta$. Besides, $\Delta f_{(m-1)mx,(m-1)my}$ stands for frequency detuning

between two VCSELs ($\Delta\varpi_{(m-1)mx,(m-1)my} = 2\pi\Delta f_{(m-1)mx}$), and $\Delta f_{(m-1)mx,(m-1)my} = \Delta f$. The above rate equations are numerically solved using the second-order Runge-Kutta method, and the time step is 2 ps [34].

The Santa-Fe chaotic time series prediction task is used to measure the prediction performance of the hierarchical time-delay RC system based on cascaded VCSELs. The Santa-Fe data set is recorded from the output of a far-infrared laser working in a chaotic state during the experiment, and it contains 9000 sample points [35]. The goal of the Santa-Fe chaotic time series prediction task is to predict the next sample under the current sample situation, that is, one-step forward prediction. The normalized mean square error (NMSE) can be used to quantitatively evaluate the performance of this task [34]:

$$\mathrm{NMSE} = \frac{\langle \|Y(h) - \bar{Y}(h)\| \rangle}{\sigma^2}, \tag{7}$$

where $\bar{Y}(h)$ is the target value and $Y(h)$ is the predicted value. σ stands for the standard deviation and h is the discrete time index. Besides, $\langle\cdot\rangle$ ($\|\cdot\|$) is the average (the norm). For the Santa-Fe chaotic time series prediction task, NMSE = 1 represents that the RC system is completely unable to predict the next output of the chaotic sequence; NMSE = 0 represents that the RC system can accurately predict the next output of the chaotic sequence. Generally speaking, NMSE $\leqslant$ 0.1 means that the prediction performance of the RC system can be considered good [34].

In the numerical simulation, the parameter values in VCSELs are as following: $\gamma_p = 10$ ns^{-1}, $\gamma_N = 1$ ns^{-1}, $\gamma_s = 50$ ns^{-1}, $|\varepsilon_0| = \frac{2}{5}$, $\Phi_0 = 0$, $\Delta f = 0$ GHz, $\Delta f_s = -5$ GHz [33]. Besides, the number of virtual nodes in each reservoir layer is $Z = 50$, the interval of virtual nodes is $\theta = 10$ ps, so the time of information processing is $T = 0.5$ ns. Thus, we set $\tau_d = \tau = T = 0.5$ ns [25]. In addition, the training set and the test set of the Santa-Fe chaotic time series prediction task each contain 1000 data points.

3 Numerical results and discussions

Firstly, the prediction performances of the hierarchical time-delay RC system based on cascaded VCSEL under different reservoir layers have been compared by numerical simulation. Here, taking one to four reservoir layers as an example, the values of NMSE as a function of the normalized injection current μ are shown in Figure 2. Note, the NMSE values shown in the following are the mean values over 5 runs, and the vertical bars are employed to represent the standard deviation around the mean value. Here, $k_{\mathrm{inj}} = 100$ ns^{-1} and $k_d = k_r = 5$ ns^{-1} are fixed. Obviously, for all the considered cases, the values of NMSE first fluctuate around a low value in a large range with the increase of μ, which means that the prediction performance remains good. With the further increase of μ, the values of NMSE increase sharply because the outputs of VCSELs become unstable [22, 25]. Combined with the inset in Figure 2, as the number of reservoir layers increases, it can be clearly observed that the values of NMSE decrease successively within the range of $\mu \subseteq [1, 1.5]$, which means that the prediction performance is gradually improved. Specifically, when there is only one reservoir layer, the value of NMSE fluctuates around 0.02; when there are two reservoir layers, the value of NMSE fluctuates around 0.018; when there are three reservoir layers, the value of NMSE fluctuates around 0.015; when there are four reservoir layers, the value of NMSE fluctuates around 0.014. The results show that, within the number of reservoir layers we considered, the hierarchical time-delay RC system based on cascaded VCSEL can obtain better prediction performance as the number of reservoir layers increases.

In the following part of this section, we only focus on the hierarchical time-delay RC system based on cascaded VCSELs with four reservoir layers. Figure 3 shows the impact of the coupling strength between VCSELs in the reservoir layers on the prediction performance. Here, $k_{\mathrm{inj}} = 100$ ns^{-1}, $\mu = 1.1$ are fixed. As presented in Figure 3(a), when $k_d = 5$ ns^{-1}, the value of NMSE decreases linearly with the increase of k_r when $k_r \subseteq [0, 10]$ ns^{-1}, and reaches the lowest value at NMSE ≈ 0.0105. When $k_r \subseteq [10, 30]$ ns^{-1}, the value of NMSE generally increases with the increase of k_r. Besides, we also consider the case of $k_d = 10$ ns^{-1}. In Figure 3(b), a similar trend can be observed, and the value of NMSE first decreases and then increases with increasing of k_r. That is to say, a medium k_r is desired to obtain enhanced prediction performance of the hierarchical time-delay RC system based on cascaded VCSELs.

The feedback strength of VCSEL in each reservoir layer is also a key factor for the prediction performance of such hierarchical RC systems. Then, the variation of NMSE with the feedback strength k_d is provided in Figure 4. Besides, we set $k_{\mathrm{inj}} = 100$ ns^{-1}, $\mu = 1.1$. Here, two cases of $k_r = 5$ ns^{-1} and $k_r =$

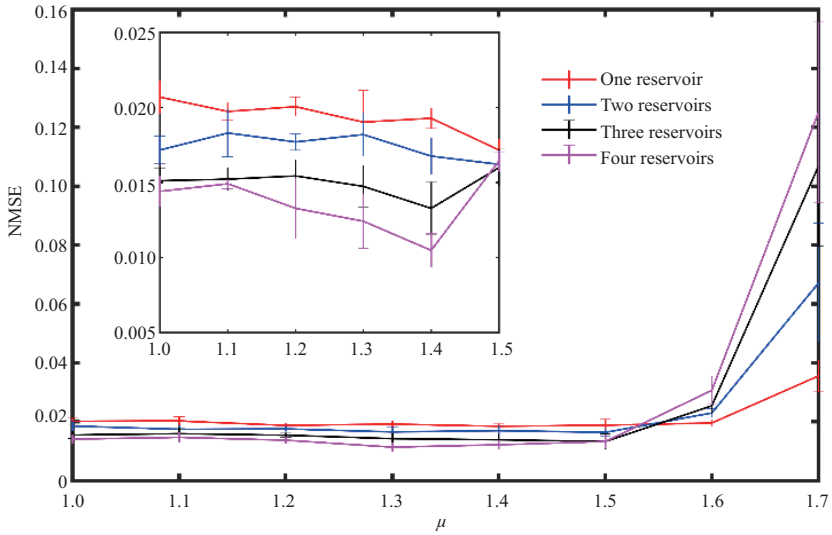

Figure 2 (Color online) Comparison of the prediction performance of the hierarchical time-delay RC systems based on cascaded VCSELs under different reservoir layers, with $k_{\text{inj}} = 100$ ns^{-1}, $k_d = k_r = 5$ ns^{-1}.

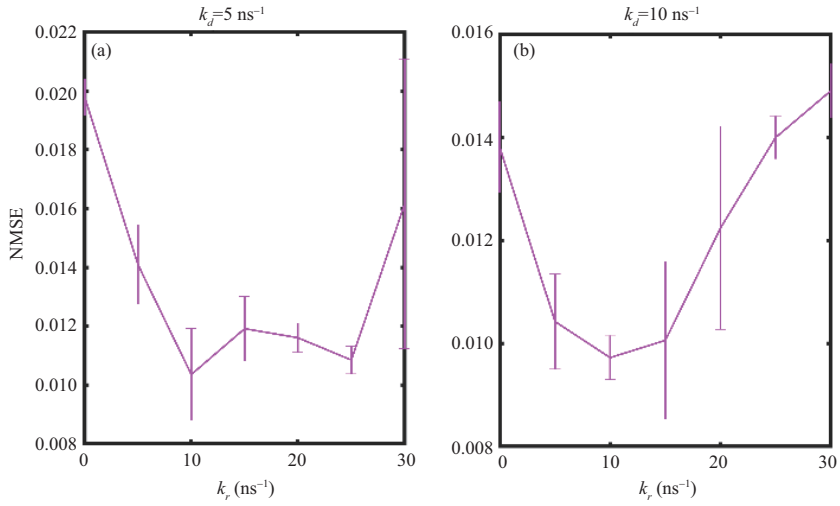

Figure 3 (Color online) NMSE values of the hierarchical time-delay RC systems based on cascaded VCSELs as a function of the coupling strength k_r for (a) $k_d = 5$ ns^{-1}, (b) $k_d = 10$ ns^{-1}, with $k_{\text{inj}} = 100$ ns^{-1} and $\mu = 1.1$.

10 ns^{-1} are taken into account, respectively. On one hand, as shown in Figure 4(a), when $k_r = 5$ ns^{-1}, in the interval of 0 ns^{-1} $\leqslant k_d \leqslant$ 20 ns^{-1}, the value of NMSE first decreases slowly with the increase of k_d, and then increases sharply with the further increasing of k_d. On the other hand, as shown in Figure 4(b), when $k_r = 10$ ns^{-1}, a similar trend can obviously be observed, and the value of NMSE gradually decreases with increasing of k_d in the interval of 0 ns^{-1} $\leqslant k_d \leqslant$ 15 ns^{-1}. When $k_d >$ 15 ns^{-1}, the value of NMSE increases sharply. It is indicated that a better prediction performance can be obtained by using lower k_d.

To further identify the regions in the parameter space of the feedback strength k_d and the coupling strength k_r contributing to better RC performance under different injection current μ, the two dimensional maps of the NMSE are provided in Figure 5. To better distinguish the regions of NMSE in Figures 5(a)–(c), the contour line NMSE = 0.012 divides the parameter space into region A corresponding to NMSE $\leqslant$ 0.012, and region B corresponding to NMSE $>$ 0.012. Here, $\mu = 1.1$, $\mu = 1.2$ and $\mu = 1.3$ are considered. Obviously, the region A narrows as μ increases. Besides, a medium k_r and lower k_d lead to a lower value of NMSE. In brief, the optimal parameters (μ, k_r, k_d) correspond to the edge of chaos [15, 19, 24, 25]. The reason is that tuning the dynamics of the RC system toward the edge of chaos provides a good compromise of the separation property and fading memory property, and then better RC performance can be obtained [36].

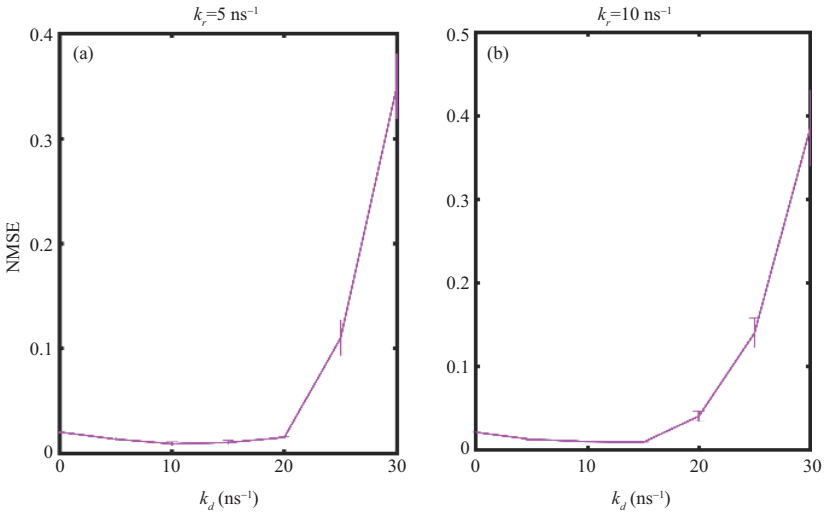

Figure 4 (Color online) NMSE values of the hierarchical time-delay RC systems based on cascaded VCSELs as a function of the feedback strength k_d for (a) $k_r = 5$ ns^{-1}, (b) $k_r = 10$ ns^{-1}, with $k_{\rm inj} = 100$ ns^{-1} and $\mu = 1.1$.

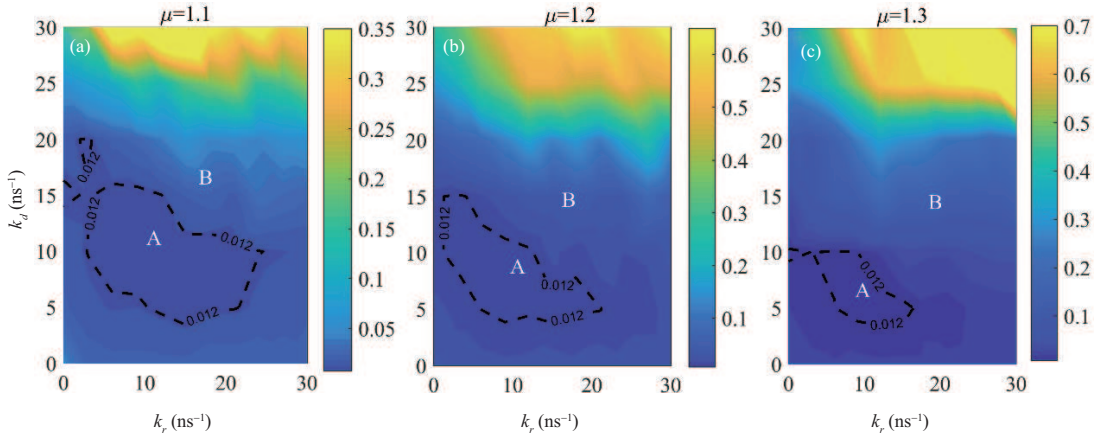

Figure 5 (Color online) Two dimensional maps of the NMSE values of the hierarchical time-delay RC systems based on cascaded VCSELs in the parameter space of k_d and k_r, with (a) $\mu = 1.1$, (b) $\mu = 1.2$, (c) $\mu = 1.3$.

Besides, the NMSE values of the hierarchical time-delay RC systems based on cascaded VCSELs as a function of the spontaneous emission factor β are further presented in Figure 6. For $k_r = 5$ ns^{-1}, as in Figure 6(a), the curves generally present an increase trend with the increment of β. In addition, the values of NMSE < 0.1 are obtained in all the considered β. For $k_r = 10$ ns^{-1}, as presented in Figure 6(b), similar trends can also be observed, which agrees with the findings obtained in [24].

For the sake of generality, we further consider the impact of the number of reservoir layers on the prediction performance of the hierarchical time-delay RC system based on cascaded VCSELs. Here, we consider the number of reservoir layers from 1 to 30. Figure 7 shows that the NMSE value of the hierarchical time-delay RC system based on cascaded VCSELs decreases as the number of the reservoir layers increases when the number of the reservoir layers changes from 1 to 8. Then, as the number of reservoir layers further increases, the value of NMSE saturates and fluctuates around 0.0135. This trend indicates that the prediction performance of the hierarchical time-delay RC system based on cascaded VCSELs can be improved within a certain range of the number of reservoir layers.

4 Experimental results

Considering the existing fiber optics platform, we propose an experimental scheme of the hierarchical time-delay RC system based on cascaded VCSELs with two reservoir layers (the idea of space division multiplexing may be used for realizing more reservoir layers). The experimental setup of such a hierar-

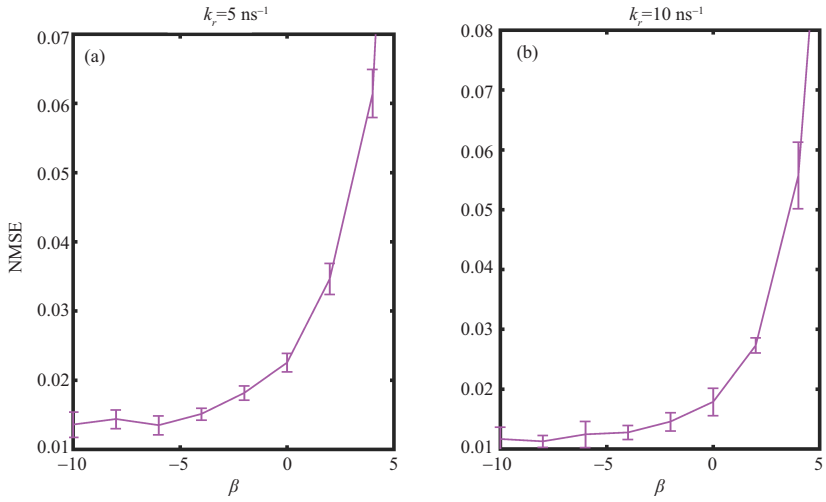

Figure 6 (Color online) NMSE values of the hierarchical time-delay RC systems based on cascaded VCSELs as a function of the spontaneous emission noise β for (a) $k_r = 5$ ns^{-1}, (b) $k_r = 10$ ns^{-1}, with $k_{\rm inj} = 100$ ns^{-1}, $k_d = 10$ ns^{-1}, and $\mu = 1.1$.

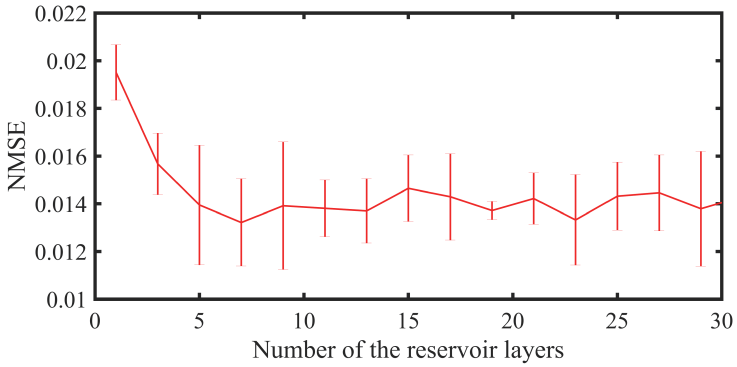

Figure 7 (Color online) NMSE values of the hierarchical time-delay RC systems based on cascaded VCSELs as a function of the number of reservoir layers, with strength $k_r = 5$ ns^{-1}, $k_d = 5$ ns^{-1}, $k_{\rm inj} = 100$ ns^{-1} and $\mu = 1.1$.

chical time-delay RC system is presented in Figure 8. Here, two commercially available 1550 nm VCSELs (SEOULVIOSYS) are used. The two VCSELs are driven by two high-stability and low-noise laser diode controllers (LDC, ILX-Lightwave LDC-3724C), respectively, which provide the injection current and allow a constant temperature operation. The experimental scheme mainly comprises three parts: (1) VCSEL1 with self-feedback light as the first reservoir layer; (2) VCSEL2 with light coupling from VCSEL1 and self-feedback light as the second reservoir layer; (3) external signal injection from an arbitrary waveform generator (AWG, Tektronix AWG70002B).

In the first reservoir layer, the emission of the VCSEL1 is divided into two parts. One part of the output is sent back to the VCSEL1, and the feedback loop is implemented by an optical circulator (CIR). Along the feedback loop, the light passes through the polarization controller (PC), which adjusts the feedback polarization. Then, through the optical fiber coupler (OC), 10% of the VCSEL1 output enters the feedback loop. Next, after the feedback light passes through the 10:90 OC, 10% and 90% of the feedback light are measured by an optical power meter (PM) and fed back to the VCSEL1, respectively. Besides, the fiber delay line (DL) and the fixed fiber length due to the packaging of each optical component are used to control the feedback delay. Here, we control the total feedback delay τ_d to be 100 ns. Furthermore, after being amplified by an erbium-doped optical fiber amplifier (EDFA), the other part of the output of VCSEL1 is coupled to the VCSEL2 by OC.

In the second reservoir layer, the emission of the VCSEL2 is also divided into two parts. One part of the output is also fed back to the VCSEL2, and the feedback loop is similar to that of the first reservoir layer. The other part of the output is first amplified by an EDFA and converted into an electrical signal by a photodetector (PD, Agilent/HP 11982A), which can be observed and recorded by an oscilloscope (OSC, Agilent DSOV334A, bandwidth 33 GHz, maximum sampling rate 80 GSa/s). Finally, the recorded

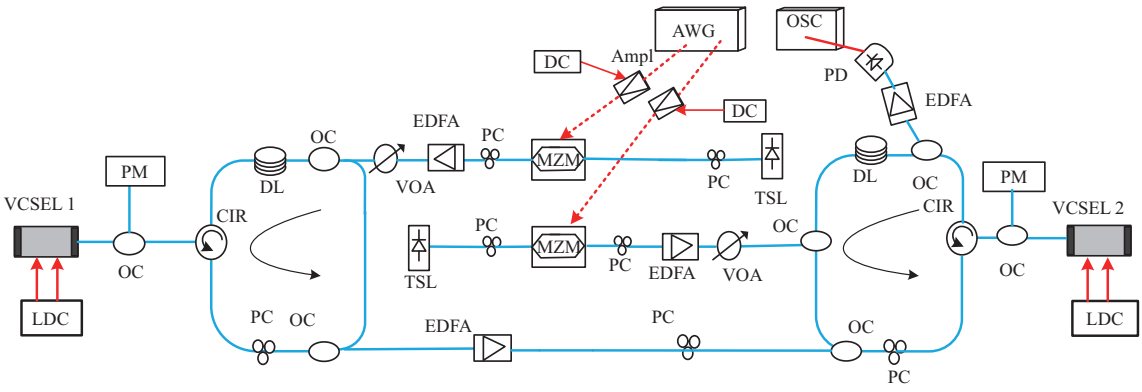

Figure 8 (Color online) Experimental setup of the hierarchical time-delay RC systems based on cascaded VCSELs with two reservoir layers. VCSEL1, VCSEL2: two vertical cavity surface emitting lasers; DC: direct current source; OSA: optical spectrum analyzer.

output time series can be used for post-processing.

In the third part, the mask input signal for the two reservoir layers is set to be consistent, and the binary mask signal $(-1, 1)$ is used. After being preprocessed in a computer, the masked input signals are encoded into the AWG and generated at a speed of 10 GSa/s from two channels of the AWG. For the first reservoir layer, one of the two generated input signals is amplified by an electric amplifier (Ampl). Next, the generated input signal is sent to the radio frequency port of the MZM. The MZM used in the experiment modulates the output of a tunable semiconductor laser (TSL) that matches the wavelength of the VCSEL1 output. The TSL output passes through two PCs in turn. The first PC is used for adjustment to align with the modulation axis of the MZM. The second PC is adopted to control the polarization of the input signal. The injected optical power of the external input signal is regulated by a variable optical attenuator (VOA) and EDFA.

Considering the bandwidth limitation of the existing AWG, combined with the frequency of the OSC and MZM, the virtual node interval θ is set to be 100 ps, and the information processing time (single data injection time) T is set to be 100 ns, which is equal to the feedback delay τ_d. Here, for computational efficiency, for every 20θ, a virtual node is sampled for post-processing. Thus, the number of virtual nodes is $M = \frac{T}{20\theta} = 50$. Besides, the threshold currents of the VCSEL1 and VCSEL2 are 2.63 and 2.12 mA, and their temperatures are set to 24.6°C and 25.65°C, respectively. Also, the bias currents of the VCSEL1 and VCSEL2 are set to 2.86 and 2.3 mA, respectively, which is 1.1 times that of the threshold current.

The optical spectra of the free-running VCSEL1 are shown in Figure 9(a). Obviously, there are two significant peaks. The peaks on the left and right are defined as the XP (wavelength of 1547.720 nm) and YP (wavelength of 1548.01 nm) modes, respectively. Evidently, the XP and YP modes are the dominant and suppression modes, respectively. Furthermore, the optical spectra of the VCSEL2 with the injections of the external input signal and VCSEL1 are shown in Figure 9(b). It can be observed that both the external input signal and the output of the VCSEL1 are injected into the XP mode of the VCSEL2, indicating that there is almost no frequency detuning between the XP modes of the VCSEL1 (the external input signal) and VCSEL2. Besides, the YP mode is suppressed.

When the power of external input signal is 300 μw and the coupling power from VCSEL1 to VCSEL2 is 25 μw, the prediction performance of the hierarchical time-delay RC system based on cascaded VCSELs is analyzed in Figure 10. The time series of the input signal is displayed in Figure 10(a), and the corresponding output series of the VCSEL2 is shown in Figure 10(b). It can be observed that the time series of the input signal and the output of the VCSEL2 have similar contours, and the output series of the VCSEL2 are more complex. Besides, the predicted value and target value of Santa-Fe chaotic time series are shown in Figures 10(c) and (d), respectively. It can be observed that the predicted value basically coincides with the target value, and NMSE is 0.0241. The results show that the hierarchical time-delay RC system based on cascaded VCSELs can successfully realize the chaotic time series prediction task.

In addition, the effect of the coupling power from VCSEL1 to VCSEL2 on the prediction performance of the hierarchical time-delay RC system based on cascaded VCSELs is considered. Here, three cases of power of external input signal are taken into account in Figure 11. For the power of external input signal fixed at 90 μw shown in Figure 9(a), when the coupling power from VCSEL1 to VCSEL2 is between 0 to 15 μw, the value of NMSE decreases as the coupling power increasing. Then when the coupling

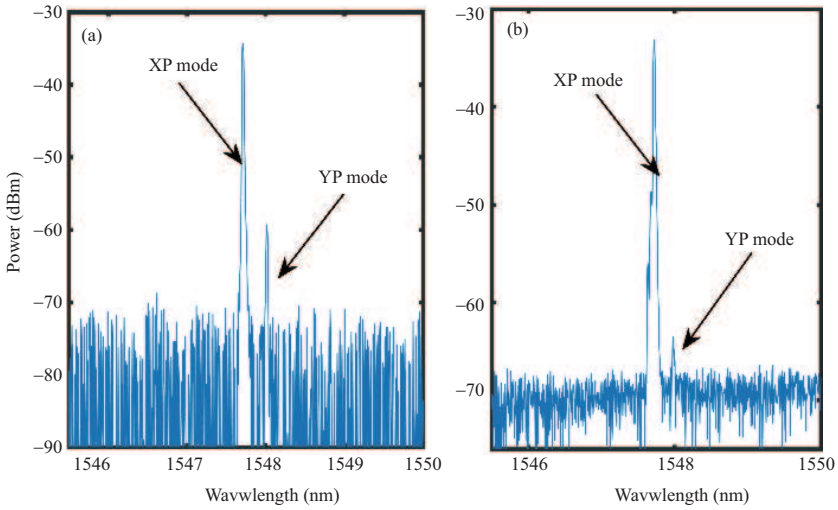

Figure 9 (Color online) (a) Optical spectra of the free-running VCSEL1; (b) optical spectra of the VCSEL2 with injection both of external input signal and VCSEL1.

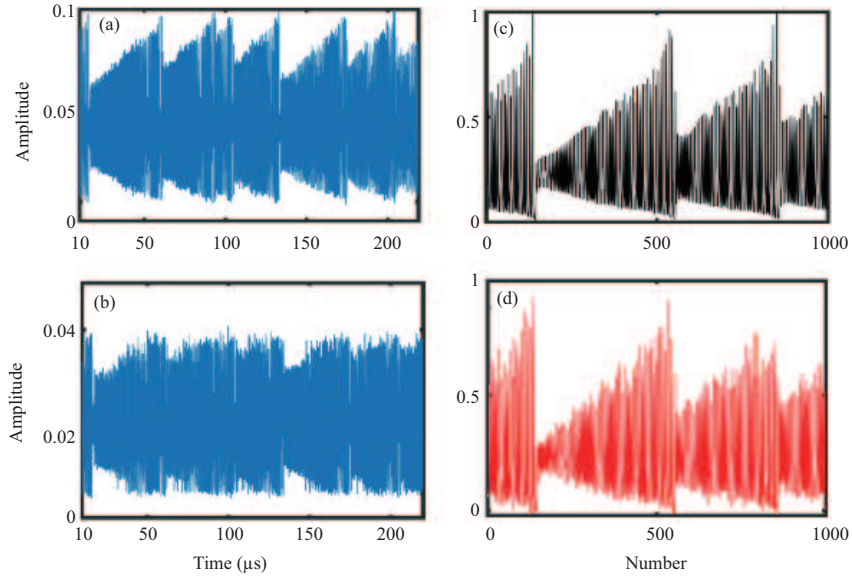

Figure 10 (Color online) Time series of (a) the input signal and (b) the VCSEL2; (c) target value and (d) predicted value for the Santa-Fe chaotic time series prediction task.

power is between 15 to 40 μw, the value of NMSE increases as the coupling power increasing, which is consistent with the numerical results in Figure 3. When the power of external input signal is fixed at 180 μw (300 μw), similar results can be observed in Figure 11(b) (Figure 11(c)), the value of NMSE first decreases then increases with the increase of the coupling power. Besides, the value of NMSE is lower than 0.1, which meaning that good prediction performance can be obtained for all the considered coupling power.

We also consider the impact of the power of external input signal on the prediction performance of the hierarchical time-delay RC system based on cascaded VCSELs. Here, two cases of coupling power from VCSEL1 to VCSEL2 are considered, 10 and 20 μw, respectively. When the coupling power is 10 μw, within the considered power range of the external injection signal, the NMSE value generally decreases with the increase of the external injection power in Figure 12(a). This is because a large external injection power can achieve injection locking, which helps the hierarchical time-delay RC system to maintain a steady state. When the coupling power is 20 μw, similar results can also be obtained in Figure 12(b). It means that the hierarchical time-delay RC experiment system can achieve high-quality prediction performance for chaotic time series tasks within a wide range of the external input signal power.

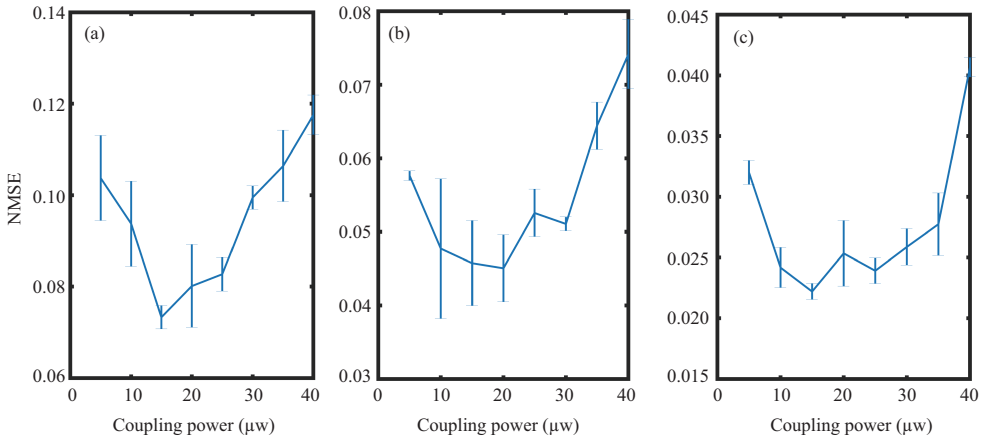

Figure 11 (Color online) NMSE values of the deep time-delay RC systems based on cascaded VCSELs with two reservoir layers as a function of the coupling power for three cases of power of external input signals (a) 90 μw, (b) 180 μw, (c) 300 μw.

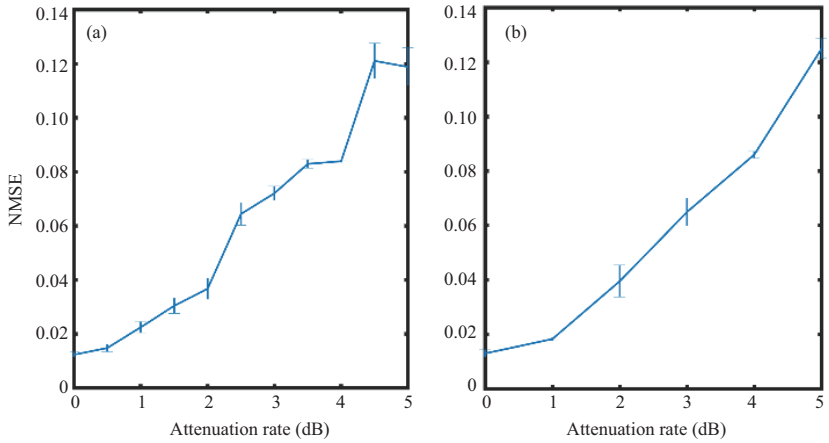

Figure 12 (Color online) NMSE values of the hierarchical time-delay RC systems based on cascaded VCSELs with two reservoir layers as a function of the external injection power for (a) 10 μw, (b) 20 μw.

5 Conclusion

Herein, we novelly propose a hierarchical time-delay optical RC system based on the cascaded VCSELs. Here, a reservoir layer is constructed by a VCSEL with feedback, and several such reservoir layers are stacked between the input and output layers. Such a proposed RC system is demonstrated numerically and experimentally. It is found that the hierarchical time-delay optical RC system can successfully complete the Santa-Fe chaotic time-series prediction task and the Mackey Glass time-series prediction (not shown here). For the numerical analysis, we have compared the prediction performance characteristics of the hierarchical time-delay RC system based on the VCSEL with one to four reservoir layers. The results show that the prediction performance of the hierarchical RC system improves as the number of reservoir layers increases. However, the prediction performance saturates when the number of reservoir layers expands to 30. Besides, the influences of the coupling strength, feedback strength, and spontaneous emission noise on the prediction performance of the hierarchical time-delay RC system based on cascaded VCSELs are considered, and we find that a medium coupling strength and a lower feedback strength are desired to obtain better prediction performance. Meanwhile, excellent RC performance can be achieved in a large spontaneous emission noise range. Additionally, an experimental setup of the hierarchical time-delay RC system based on cascaded VCSELs with two reservoir layers is introduced and investigated. The impact of the coupling power has been considered. It is also found that better prediction performance can be observed with medium coupling power, which agrees well with the numerical analysis. We also find that a larger external input signal power helps improve the prediction performance from the experimental results. Also, the proposed hierarchical RC system can realize the depth in time and has the potential to realize the depth in space. Thus, the hierarchical RC system can guide subsequent deep RC systems

and may be beneficial in improving the complex problem-solving ability of RC systems.

Acknowledgements This work was supported in part by National Key Research and Development Program of China (Grant Nos. 2021YFB2801900, 2021YFB2801901, 2021YFB2801902, 2021YFB2801903, 2021YFB2801904), National Outstanding Youth Science Fund Project of National Natural Science Foundation of China (Grant No. 62022062), National Natural Science Foundation of China (Grant Nos. 62204196, 61974177, 61674119), and Key Lab of Modern Optical Technologies of Jiangsu Province, Soochow University (Grant No. KJS2140).

References

1 Merolla P A, Arthur J V, Alvarez-Icaza R, et al. A million spiking-neuron integrated circuit with a scalable communication network and interface. Science, 2004, 345: 668–673
2 Poo M, Du J, Ip N Y, et al. China brain project: basic neuroscience, brain diseases, and brain-inspired computing. Neuron, 2016, 92: 591–596
3 Wang R, Ren Q S, Zhao J Y. Research progress on photonic neuromorphic computing. Laser Optoelectron Prog, 2016, 53: 120004
4 Verstraeten D, Schrauwen B, D'Haene M, et al. An experimental unification of reservoir computing methods. Neural Netw, 2007, 20: 391–403
5 Hinaut X, Lance F, Droin C, et al. Corticostriatal response selection in sentence production: insights from neural network simulation with reservoir computing. Brain Language, 2015, 150: 54–68
6 Cucchi M, Gruener C, Petrauskas L, et al. Reservoir computing with biocompatible organic electrochemical networks for brain-inspired biosignal classification. Sci Adv, 2021, 7: eabh0693
7 Jaeger H, Haas H. Harnessing nonlinearity: predicting chaotic systems and saving energy in wireless communication. Science, 2004, 304: 78–80
8 Maass W. Liquid state machines: motivation, theory, and applications. In: Computability in Context: Computation and Logic in the Real World. Singapore: World Scientific, 2011
9 Cuchiero C, Gonon L, Grigoryeva L, et al. Discrete-time signatures and randomness in reservoir computing. IEEE Trans Neural Netw Learn Syst, 2022, 33: 6321–6330
10 Zhong Y, Tang J, Li X, et al. Dynamic memristor-based reservoir computing for high-efficiency temporal signal processing. Nat Commun, 2021, 12: 408
11 Appeltant L, Soriano M C, van der Sande G, et al. Information processing using a single dynamical node as complex system. Nat Commun, 2011, 2: 468–473
12 Larger L, Soriano M C, Brunner D, et al. Photonic information processing beyond Turing: an optoelectronic implementation of reservoir computing. Opt Express, 2012, 20: 3241–3249
13 Guo X X, Xiang S Y, Zhang Y H, et al. Enhanced memory capacity of a neuromorphic reservoir computing system based on a VCSEL with double optical feedbacks. Sci China Inform Sci, 2020, 63: 160407
14 Sugano C, Kanno K, Uchida A. Reservoir computing using multiple lasers with feedback on a photonic integrated circuit. IEEE J Sel Top Quantum Electron, 2020, 26: 1–9
15 Hou Y S, Xia G Q, Yang W Y, et al. Prediction performance of reservoir computing system based on a semiconductor laser subject to double optical feedback and optical injection. Opt Express, 2018, 26: 10211–10219
16 Huang Y, Zhou P, Yang Y, et al. Time-delayed reservoir computing based on a two-element phased laser array for image identification. IEEE Photon J, 2021, 13: 1–9
17 Koyama F. Recent advances of VCSEL photonics. J Lightwave Technol, 2006, 24: 4502–4513
18 Xiang S, Ren Z, Zhang Y, et al. All-optical neuromorphic XOR operation with inhibitory dynamics of a single photonic spiking neuron based on a VCSEL-SA. Opt Lett, 2020, 45: 1104–1107
19 Li N, Susanto H, Cemlyn B R, et al. Stability and bifurcation analysis of spin-polarized vertical-cavity surface-emitting lasers. Phys Rev A, 2017, 96: 013840
20 Xiang S, Zhang Y, Gong J, et al. STDP-based unsupervised spike pattern learning in a photonic spiking neural network with VCSELs and VCSOAs. IEEE J Sel Top Quantum Electron, 2019, 25: 1–9
21 Ling W A, Lyubomirsky I, Rodes R, et al. Single-channel 50G and 100G discrete multitone transmission with 25G VCSEL technology. J Lightwave Technol, 2015, 33: 761–767
22 Vatin J, Rontani D, Sciamanna M. Enhanced performance of a reservoir computer using polarization dynamics in VCSELs. Opt Lett, 2018, 43: 4497–4500
23 Vatin J, Rontani D, Sciamanna M. Experimental reservoir computing using VCSEL polarization dynamics. Opt Express, 2019, 27: 18579–18584
24 Guo X X, Xiang S Y, Zhang Y H, et al. Polarization multiplexing reservoir computing based on a VCSEL with polarized optical feedback. IEEE J Sel Top Quantum Electron, 2020, 26: 1–9
25 Guo X X, Xiang S Y, Zhang Y H, et al. Four-channels reservoir computing based on polarization dynamics in mutually coupled VCSELs system. Opt Express, 2019, 27: 23293–23306
26 Tao J Y, Wu Z M, Yue D Z, et al. Performance enhancement of a delay-based reservoir computing system by using gradient boosting technology. IEEE Access, 2020, 8: 151990
27 Nguimdo R M, Lacot E, Jacquin O, et al. Prediction performance of reservoir computing systems based on a diode-pumped erbium-doped microchip laser subject to optical feedback. Opt Lett, 2017, 42: 375–378
28 Nguimdo R M, Erneux T. Enhanced performances of a photonic reservoir computer based on a single delayed quantum cascade laser. Opt Lett, 2019, 44: 49–52
29 Jiang N, Pan W, Luo B, et al. Bidirectional dual-channel communication based on polarization-division-multiplexed chaos synchronization in mutually coupled VCSELs. IEEE Photon Technol Lett, 2012, 24: 1094–1096

30 Deng T, Robertson J, Hurtado A. Controlled propagation of spiking dynamics in vertical-cavity surface-emitting lasers: towards neuromorphic photonic networks. IEEE J Sel Top Quantum Electron, 2017, 23: 1–8
31 Deng T, Robertson J, Wu Z M, et al. Stable propagation of inhibited spiking dynamics in vertical-cavity surface-emitting lasers for neuromorphic photonic networks. IEEE Access, 2018, 6: 67951–67958
32 Jiang N, Zhao A, Xue C, et al. Physical secure optical communication based on private chaotic spectral phase encryption/decryption. Opt Lett, 2019, 44: 1536–1539
33 Zhang H, Xiang S, Zhang Y, et al. Complexity-enhanced polarization-resolved chaos in a ring network of mutually coupled vertical-cavity surface-emitting lasers with multiple delays. Appl Opt, 2017, 56: 6728–6734
34 Nguimdo R M, Verschaffelt G, Danckaert J, et al. Simultaneous computation of two independent tasks using reservoir computing based on a single photonic nonlinear node with optical feedback. IEEE Trans Neural Netw Learn Syst, 2015, 26: 3301–3307
35 Weigend A S, Gershenfeld N A. Time series prediction: forecasting the future and understanding the past. Intern J Forecast, 1994, 10: 161–163
36 Tanaka G, Yamane T, Héroux J B, et al. Recent advances in physical reservoir computing: a review. Neural Netw, 2019, 115: 100–123